Design and Validation of A Multi-link Phase-Compensated Long-Range Ultrawideband VNA-based Channel Sounder

Lyu, Yejian; Mbugua, Allan Wainaina; Yuan, Zhiqiang; Olesen, Kim; Fan, Wei

Published in:
I E E E Transactions on Microwave Theory and Techniques

DOI (link to publication from Publisher):
10.1109/TMTT.2022.3194045

Publication date:
2022

Document Version
Accepted author manuscript, peer reviewed version

Design and Validation of A Multi-link Phase-Compensated Long-Range Ultrawideband VNA-based Channel Sounder

Yejian Lyu, Allan Wainaina Mbugua, Zhiqiang Yuan, Kim Olesen, and Wei Fan

***Abstract*—This paper presents a novel and cost-effective vector network analyzer (VNA)-based phase-compensated channel sounder operating in the frequency range of 10-50 GHz using radio-over-fiber (RoF) techniques, which can support multi-link/channel long-range phase-coherent measurements. The optical cable enables long-range channel measurements with a dynamic range of 115.7 dB at 30 GHz (for the back-to-back connection). The phase compensation scheme is utilized for stabilizing the inherent phase variations introduced by the optical fiber of the channel sounder to enable its application in multi-channel/antenna measurements. A novel optical delay line and combiner scheme is proposed and implemented to separate the signals, thereby saving the port resource on the VNA for multi-link/channel measurements. The proposed channel sounder is validated in back-to-back measurements under two optical cable conditions, i.e., with the presence of thermal changes and mechanical stress. The phase change could be maintained within 3° at 10-30 GHz and 7° in 30-50 GHz, respectively, compared to the over 80° phase variation introduced by the cable effects at 10-50 GHz, demonstrating the robustness and effectiveness of the developed channel sounder in practice. With the proposed optical delay line and combiner scheme, multiple channels can be measured simultaneously with minimal VNA ports, significantly reducing the measurement cost and time for multi-link channel measurements. Two multi-link indoor channel measurements are conducted and analyzed using a virtual uniform rectangular array (URA) at 28 GHz bands. The results demonstrate the capability of the proposed channel sounder to perform high-fidelity long-range ultrawideband multi-link channel measurements.**

***Index Terms*—Channel sounding, multi-link, millimeter wave, radio-over-fiber, phase compensation.**

I. Introduction

MASSIVE multiple-input multiple-output (MIMO), which can serve multiple users in the same time-frequency resource, has become a key technology for the fifth-generation (5G) and future communication systems [1]–[5]. The performance of massive MIMO highly depends on the spatial locations of the multiple users. It is thus crucial to have an accurate knowledge of the channel characteristic in target deployment scenarios.

Y. Lyu, K. Olesen, and W. Fan are with the Antenna, Propagation and Millimeter-wave Systems (APMS) Section, Department of Electronic Systems, Faculty of Engineering and Science, Aalborg University, 9220 Aalborg, Denmark (e-mail: yely@es.aau.dk; ko@es.aau.dk; wfa@es.aau.dk);

A. W. Mbugua is with the APMS Section, 9220 Aalborg, Denmark and Huawei Technologies Duesseldorf GmbH, Munich Research Center, 80992 Munich, Germany (e-mail: allan.mbugua@huawei.com);

Z. Yuan is with State Key Lab of Networking and Switching Technology, Beijing University of Posts and Telecommunications, 100876 Beijing, China (e-mail: yuanzhiqiang@bupt.edu.cn).

Corresponding author: Wei Fan.

Reliable channel sounder is fundamental for accurate channel characterization. According to [6]–[9], channel sounders require specialized hardware to achieve desired performance, e.g., flexible carrier frequency settings, scalable measurement bandwidth, high dynamic range, high sampling rate, scalable antenna configuration, etc. However, practical channel sounders cannot meet all the requirements due to the hardware and cost limitations.

Recently, the large potential and interest of massive MIMO have motivated numerous multi-link channel sounder design and measurement campaigns to investigate the multi-user channel at sub-6 GHz bands [10]–[14] and millimeter-wave (mmWave) bands [15], [16]. Generally, state-of-the-art multi-link channel sounders are based either on time-domain or frequency-domain structure. Time-domain-based channel sounders coupled with real antenna array (RAA) are typically used to investigate the massive MIMO channel with a high sampling rate and free operation of the transmitter (Tx) and receiver (Rx) [12]–[14]. However, on the other hand, the drawbacks are the limited bandwidth and the complexity of the clock synchronization between the Tx and Rx. Moreover, with an increase in the frequency and the number of the transceiver chains, the cost of the system and the complexity of the calibration increase as well [17].

The vector network analyzer (VNA) is a widely used frequency-domain channel sounder for massive MIMO investigation (using the virtual antenna array (VAA) strategy) due to its ability to support channel sounding with flexible carrier frequency setting, ultrawideband, easy calibration, easy access in radio frequency (RF) laboratories, and high dynamic range [18]–[21]. VAA is a popular and cost-effective method to measure static spatial channels, where the basic idea is that we can use a single antenna element with the help of a mechanical positioner to record the channel at multiple spatial locations (i.e. VAA elements) [15], [22]–[26]. However, the downside is that there are three limitations that constrain the use of VNA-based sounder to investigate the MIMO channels. Firstly, the measurement scenario is typically limited to the static scenarios due to the long sweeping time and possible involvement of the mechanic rotation system for spatial channel measurements. Secondly, since the signal generator and analyzer are co-located in the VNA, we need to remote antennas (i.e. extend antennas connected to VNA via cable connection) to record channel frequency response for typical deployment environment. As a result, VNA-based channel sounder is typically employed for short-range measurement

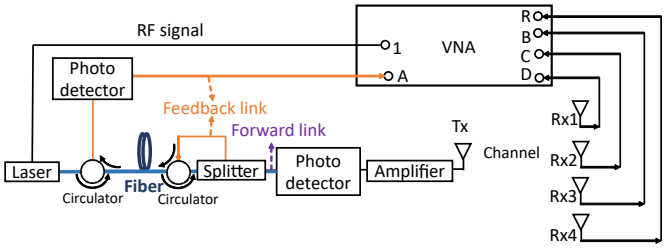

Fig. 1: Block diagram of the conventional multi-user RoF VNA-based channel sounder.

scenarios due to the reduction of the dynamic range introduced by the cable loss on the RF cable, especially at mmWave band. The third limitation is the limiting port resource on the VNA, which limits the number of the transceiver chains in the sounding system [27], [28].

Several solutions were reported to mitigate the static scenario limitation with the VNA. Firstly, the frequency sweeping time in the VNA could be reduced by increasing the intermediate frequency (IF) bandwidth in the VNA, at the cost of reduced system dynamic range. Furthermore, multiple static snapshots of the channels over several spatial locations could be measured to mimic dynamic propagation environments [29], [30]. Moreover, in principle, if the dominant scatterers in the propagation environment remain static, the VAA concept can still be employed in practice, as demonstrated in the outdoor measurements in [31].

Radio-over-fiber (RoF) techniques are typically utilized to combat the second limitation, i.e., high signal loss in the RF cables. The use of the optical fiber cables could significantly reduce the signal loss in the cables (e.g. 0.4 dB/km for a single-mode optical fiber [32] compared to approximately 1.59 dB/m for a coaxial cable at 30 GHz [33]). However, the phase of the signal in the fiber is inherently sensitive to the thermal change and mechanical stress of the fiber cables [34], [35], limiting its application for phase-coherent measurements, e.g., VAA-based channel measurements, which is widely used for spatial channel measurements at mmWave bands [15]. To enable phase-coherent ultrawideband channel measurements in the long-range scenarios, phase compensation strategies were presented in [19], [20], [36], [37]. The phase compensation scheme using the bidirectional strategy was applied in the VNA-based channel sounder using RoF techniques up to 30 GHz in [19] and extended to 50 GHz in [37]. Furthermore, the phase compensation scheme is extended to sub-THz frequency bands, i.e., 220-330 GHz in [20] and compensated phase variation is up to 15° compared to over 400° before phase compensation. The results in the literature demonstrate the effectiveness of the phase compensation strategy for VNA-based channel sounders.

The third limitation of the VNA-based channel sounder could be solved by two schemes, i.e., fast switch enabled scheme and optical delay line and combiner scheme. In [38], a fast switch enabled massive MIMO scheme is proposed, which could significantly reduce the complexity and cost of the transceiver chains. Nonetheless, this fast switch enabled channel sounder cannot measure the multiple chains simultaneously. For optical delay line and combiner solution, the combiner is used to combine multi-link signals to save VNA ports. To maintain the orthogonality of the combined multi-link signal, we could apply delay lines, where signals can be delayed by L_{delay}/c_{fiber} with L_{delay} and c_{fiber} denoting the length of the optical delay line and the speed of light in fiber, respectively. Preliminary channel impulse response (CIR) results in [39] indicate the multiple channels could be measured simultaneously in one port at sub-6 GHz bands. However, the unstable phase performance of the signals in the delay line at higher frequency bands (e.g. mmWave) limits the use of this scheme in phase-coherent measurements. Furthermore, the cost of the RoF scheme also becomes problematic when the delay line and combiner concept is directly extended for the mmWave bands. Besides, in sub-6 GHz frequency bands, the system response of the RoF scheme is rather insignificant, and therefore system calibration is not important and omitted in [39]. [39].

In this paper, we aim to realize a multi-link channel sounder that could achieve long-range phase-coherent measurements with minimal VNA ports. In this proposed channel sounder, RoF techniques are utilized to extend the measurement range, the down-conversion scheme is applied to down-convert the mmWave signal to lower frequency bands (i.e. 10-60 MHz), whose phase change introduced by the fiber cables is insignificant [40] and could use delay line strategy to combine multiple received signals into one port, which saves the port resource of the VNA. As discussed in Section III-D, by using suitable optical delay lines, splitter, and combiner, we could achieve channel measurements of up to N Rx links using 3 receiving ports (Port A for Tx reference signal, Port B for Rx signal, and Port C for phase compensation). The use of the low frequency (LF)[1] RoF units also reduce the cost of the sounder. Besides, since the multiple system responses and channel responses are mixed by the combiner, the simple calibration method, i.e. transmission normalization, cannot be applied to this proposed sounder, i.e. recording the system response in the back-to-back connection and then directly normalizing it to the received frequency response. Thus, a novel calibration procedure is proposed and validated.

The main contributions of this paper are summarized as follows:

- We design and validate a novel and cost-effective multi-link phase-compensated long-range VNA-based channel sounder at 10-50 GHz. Note that this proposed scheme can be applied for arbitrary frequency ranges with the components operating in the appropriate frequency bands.
- Our proposed channel sounder structure can offer fast measurement, enabled by parallel multi-link channel measurements using a delay-line and combiner scheme and a novel calibration procedure.
- Experimental validations of the link budget, the calibration scheme, and the phase compensation scheme are presented.
- Two multi-link channel measurements in indoor scenarios are presented to validate the effectiveness and robustness

[1] In this paper, LF indicates the frequency range of 0.5 MHz-6 GHz

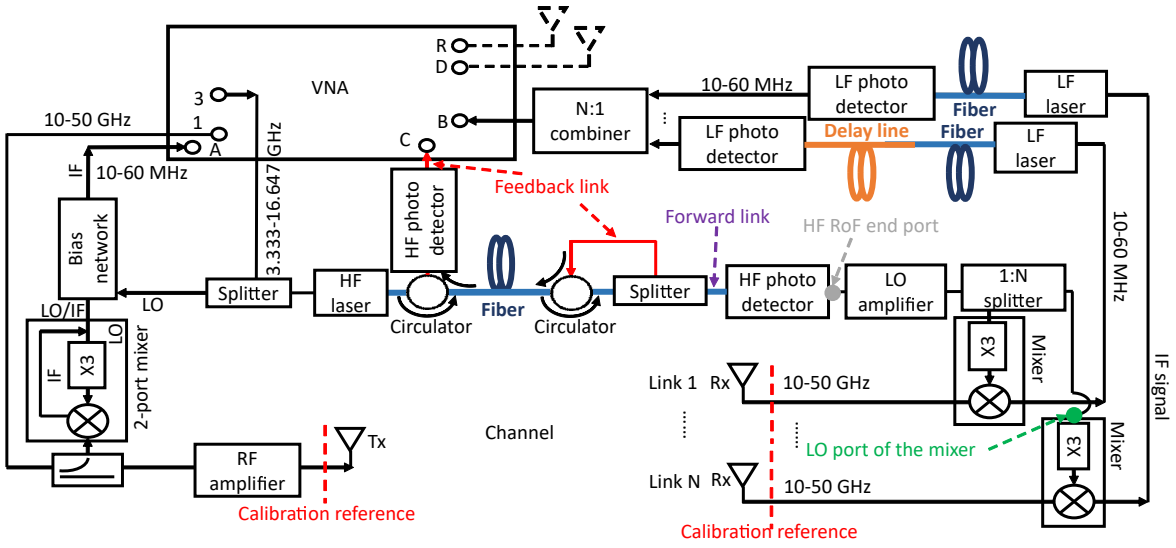

Fig. 2: Block diagram of the proposed multi-user RoF VNA-based channel sounder.

of the proposed channel sounder.

The rest of this paper is organized as follows. Section II outlines the architecture of the proposed channel sounder. Section III contains a detailed description of the validation measurements and the analysis of the results. The channel validation measurement campaigns and results are demonstrated in Section IV. Finally, concluding remarks are presented in Section V.

II. Channel Sounder Architecture

A. Sounder Architecture

Fig. 1 depicts the conventional multi-link long-range phase-compensated channel sounder, as a direct extension of the sounder in [19]. This is a simple and straightforward phase-coherent measurement enabled multi-link sounder. However, the main limitation is that the port resource is limited for commercial VNAs. In the commercial four-port VNA, Keysight N5227B, it has 4 ports, i.e. Port 1-4, for both transmitting and receiving signals. Besides, it also has 5 receiving ports, i.e. Port A-D and R. Port R is switched to receive the transmitted signal from Port 1-4, while Port A-D serves to receive the received signal from Port 1-4. Thus, using the multi-link sounder in Fig. 1 means that the maximum number of the Rx links can only reach 4 (one port for phase compensation). Optical delay line and combiner scheme could be a solution for saving the port resource. However, the scheme cannot be directly applied to higher frequency bands due to the unstable phase performance of the signals in the delay lines. Thus, in order to save the port resource, extend the number of Rx links, and perform phase-coherent measurement, a multi-link channel sounder with a novel optical delay line and combiner scheme is proposed in this work.

Fig. 2 and Fig. 3 illustrate the block diagram of the proposed channel sounder and the photo of the sounding system, respectively. The types and working frequencies of the main channel sounder components are outlined in Table I. RF signal at 10-50 GHz is transmitted from Port 1 and divided into

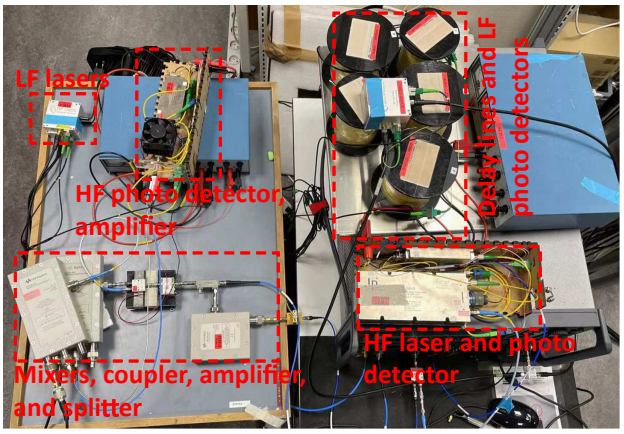

Fig. 3: Photo of the proposed channel sounder in the back-to-back connection.

two signals by a coupler. One of the split signals is used to transmit through an antenna and the other is used to generate 10-60 MHz reference signal. The 3.333-16.647 GHz local oscillator (LO) signal is transmitted by Port 3 and split into two signals. The split LO signal is sent to the mixers. Note that the LO of the mixer operates at the third harmonic. At the Rx side, multiple Rx links are applied and the received signals are down-converted to an intermediate frequency (IF), i.e., 10-60 MHz with the help of the mixer.

The LF RoF units, i.e., LF laser, fiber, and LF photo detector are used on the IF signal to remote the Rx antennas and reduce the signal loss on the cables. Eventually, the received signals are combined by a combiner and sent to Port B.

The main benefits of the proposed systems are that multiple channels can be simultaneously measured with only one VNA receiving port, which leads to significantly reduced measurement time and cost for multi-link measurements. With the proposed structure, multiple parallel Rx channels working at the same frequency range will be received at Port B and we need to separate the signals for the multiple channels

in post-processing. In this work, a novel optical delay line and combiner scheme is proposed to achieve this purpose. Due to the lack of the RF components in our laboratory, e.g. mixers, in the following validation and channel measurement part, we only apply 2 Rx links with two 3-ports mixers at the Rx side as an example. Note that the proposed principle can be directly applied to multi-user scenarios. The IF signal bandwidth is limited to 10-60 MHz in the proposed system due to the 2-port mixer and bias network employed in the Tx side. This, however, is not a limitation in principle for the proposed system. Note that the IF signal bandwidth is the bandwidth of the 10-60 MHz IF signal, and the VNA IF bandwidth refers to the IF bandwidth in the VNA.

TABLE I: Main components of the proposed channel sounder

Part	Name	Frequency/Wavelength
Sounding and down-conversion part		
VNA	Keysight PNA N5227B	0.01-67 GHz
Coupler	Keysight 87301E	2 MHz-50 GHz
Mixer	Keysight 85320A-H50	2-50 GHz
Mixer	Ketsight 85320B-H50	2-50 GHz
Bias Network	Keysight 11612B	45 MHz-50 GHz
RF amplifier	CBM26402520	26.5-40 GHz
Tx antenna	Custom wideband biconical antenna [41]	1.5-40 GHz
Rx antenna	AINFO-SZ-2003000/P	2-30 GHz
Phase compensation scheme		
HF laser	QMOD XMTQ-C-A-24	1550 nm
HF photo detector	QMOD XMRQ-C-A-24	1550 nm
Optical splitter	JDS FFC-CKH12B105-003	1550 nm
Optical circulator	OZ FOC-12N-111-9/125-SSS -1550-55-SCASCASCA-1-1	1550 nm
LO amplifier	AMF-KD-02001800-29-20P	2-18 GHz
LF RoF scheme		
LF laser	RFoF6T3FR-PA-11	0.5 MHz-6 GHz
LF photo detector	RFoF6R3FR-PA-11	0.5 MHz-6 GHz

B. Principle of Phase Compensation

The phase compensation scheme is applied on the Rx LO side to remote the Rx antenna and guarantee the stable system phase. The phase compensation scheme has been proposed in [19] and extensively validated. Here, only the basic idea is explained. A high frequency (HF)[2] optical fiber link with a frequency range of 1-50 GHz is used for the forward link. An optical power splitter is used to divide equally the optical signal between the forward and feedback links, which results in a power loss of 6 dB at each port. Two non-polarization-maintaining three-port optical circulators are used to enable bidirectional signal transmission on the same single-mode optical cable. Using the feedback link, the inherent random phase variation introduced by the optical fiber is fed back to VNA and recorded in Port C.

The forward link and feedback link are recorded in the VNA as the S-parameter $S_{\mathrm{BA}}(f_1)$ and $S_{\mathrm{C3}}(f_2)$, respectively, where f_1 ranges from 10 MHz to 60 MHz, and f_2 ranges from 3.333 GHz to 16.647 GHz with the same amount of frequency points. Since the LO of the mixer operates at the third harmonic, the relationship between the RF frequency f, which ranges from 10-50 GHz, IF frequency f_1, and LO frequency f_2 could be formulated as:

$$f_1 = f - f_2 \cdot 3 \tag{1}$$

Replacing the back-to-back connection with suitable antennas in the actual channel measurements, the frequency response $S(f_1)$ can be recorded in $S_{\mathrm{BA}}(f_1)$ as:

$$S_{\mathrm{BA}}(f_1) = H_{\mathrm{fw}}(f_1) \cdot S(f_1), \tag{2}$$

where $H_{\mathrm{fw}}(f_1)$ denotes the frequency response caused by the mechanical stress and thermal changes on the optical fiber. Note that the frequency response $S(f_1)$ contains the multi-link channel frequency response $H_1(f_1)$, $H_2(f_1)$, ..., $H_n(f_1)$ and the system response $C_1(f_1)$, $C_2(f_1)$, ..., $C_n(f_1)$, which will be explained later in (11) and (12).

For the feedback link, the frequency response needs to be normalized before the measurements. The frequency response after normalization, which contains the cable effects, $H_{\mathrm{fb}}(f_2)$ is embedded in $S_{\mathrm{C3}}(f_2)$ as:

$$S_{\mathrm{C3}}(f_2) = 1 \cdot H_{\mathrm{fb}}(f_2) = \alpha_{\mathrm{C3}}(f_2) \exp(j\phi_{\mathrm{C3}}(f_2)), \tag{3}$$

where $\alpha_{\mathrm{C3}}(f_2)$ and $\phi_{\mathrm{C3}}(f_2)$ are the amplitude and phase of $S_{\mathrm{C3}}(f_2)$, respectively.

We define the amplitude and phase response from the HF photo detector output port in the forward link to Port 3 as $\alpha_{\mathrm{PD3}}(f_2)$ and $\phi_{\mathrm{PD3}}(f_2)$, respectively. The signal undergoes twice the phase change caused by the impairments of the optical cable, i.e. mechanical stress and thermal change, in the forward link through the bidirectional optical fiber. Thus, the relationship between $\alpha_{\mathrm{PD3}}(f_2)$ and $\phi_{\mathrm{PD3}}(f_2)$ with the amplitude and phase change of $S_{\mathrm{C3}}(f_2)$ can be calculated as:

$$\alpha_{\mathrm{PD3}}(f_2) = \sqrt{\alpha_{\mathrm{C3}}(f_2)} = \sqrt{|S_{\mathrm{C3}}(f_2)|}, \tag{4}$$

$$\phi_{\mathrm{PD3}}(f_2) = \frac{\phi_{\mathrm{C3}}(f_2)}{2}, \tag{5}$$

The amplitude and phase change through the LO amplifier and 1-N splitter is insignificant after calibration. Thus, the relationship between the amplitude $\alpha_{\mathrm{LO3}}(f_2)$ and phase $\phi_{\mathrm{LO3}}(f_2)$ of the response from the LO signal input port at the Rx side to Port 3 and $\alpha_{\mathrm{PD3}}(f_2)$ and $\phi_{\mathrm{PD3}}(f_2)$ are:

$$\alpha_{\mathrm{LO3}}(f_2) \approx \alpha_{\mathrm{PD3}}(f_2) = \sqrt{\alpha_{\mathrm{C3}}(f_2)} = \sqrt{|S_{\mathrm{C3}}(f_2)|}, \tag{6}$$

$$\phi_{\mathrm{LO3}}(f_2) \approx \phi_{\mathrm{PD3}}(f_2) = \frac{\phi_{\mathrm{C3}}(f_2)}{2}. \tag{7}$$

After passing through the $3\times$ multiplier and mixer, the amplitude $\alpha_{\mathrm{error}}(f_1)$ and phase $\phi_{\mathrm{error}}(f_1)$ of the error term $H_{fw}(f_1)$ can be written as:

$$\alpha_{\mathrm{error}}(f_1) \approx \alpha_{\mathrm{LO3}}(f_2) = \sqrt{|S_{\mathrm{C3}}(f_2)|}, \tag{8}$$

$$\phi_{\mathrm{error}}(f_1) = 3 \cdot \phi_{\mathrm{LO3}}(f_2) = 1.5 \cdot \phi_{\mathrm{C3}}(f_2), \tag{9}$$

Consequently, the error term $H_{\mathrm{fw}}(f_1)$ can be deembedded from the $S(f_1)$ as follows:

$$S(f_1) = \frac{S_{\mathrm{BA}}(f_1)}{\sqrt{|S_{\mathrm{C3}}(f_2)|} \exp(j \cdot 1.5 \cdot \phi_{\mathrm{C3}}(f_2))} \tag{10}$$

[2]In this paper, HF indicates the frequency range of 10 MHz-50 GHz

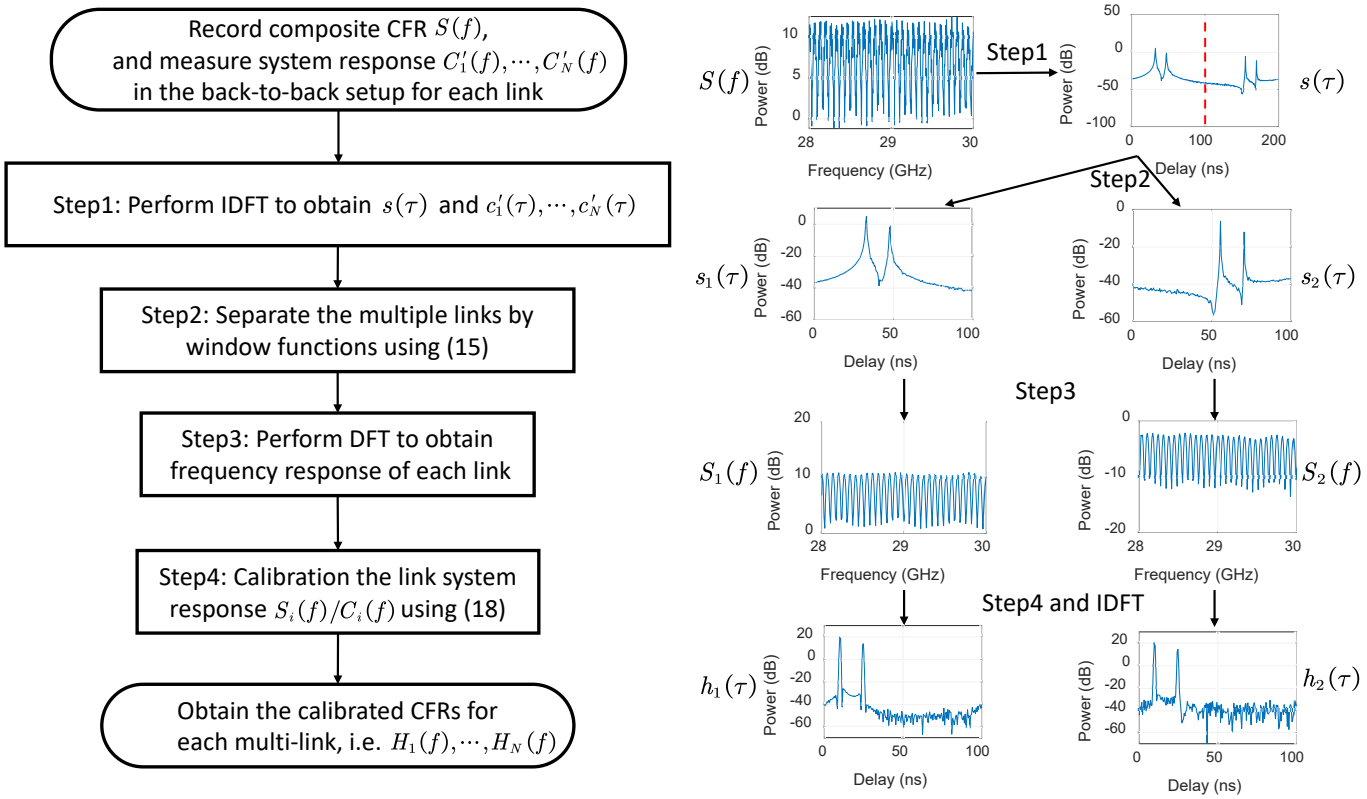

Fig. 4: Flow chart of the proposed calibration procedure.

C. Calibration Procedure

After the phase compensation procedure, in order to obtain the target channel responses, the system response needs to be de-embedded. The conventional transmission normalization method applies a normalization function to eliminate the system response in the back-to-back setup [19]. However, in our proposed channel sounder, the products of the channel frequency response and the system response are combined together, which makes the transmission normalization inapplicable to de-embed the system response as explained later. A novel calibration procedure for this channel sounder is proposed in this subsection. Fig. 4 illustrates the flow chart of our proposed calibration procedure. We also perform a simulation as a simple example to better demonstrate the calibration method. In the simulation, the channel is set to be 2 path and the delay line is 20.4 m, which corresponds to the delay of 100 ns. The detailed simulation configuration can be found in Table II.

Assume that the lengths of the optical delay lines used for Link 2, Link 3, ..., Link N are L_{delay}, $2L_{delay}$, ..., $(N-1)L_{delay}$. The frequency response of the received signal could be written as:

$$\begin{aligned} S(f_1) = S_1(f_1) + S_2(f_1)\cdot e^{-j2\pi f_1 \Delta\tau} \\ + \ldots + S_n(f_1)\cdot e^{-j2\pi f_1 (N-1)\Delta\tau} \end{aligned} \tag{11}$$

In this equation, we have

$$\begin{cases} S_1(f_1) & = H_1(f_1)\cdot C_1(f_1) \\ S_2(f_1)\cdot e^{-j2\pi f_1\Delta\tau} & = H_2(f_1)\cdot C_2(f_1) \\ & \vdots \\ S_n(f_1)\cdot e^{-j2\pi f_1(N-1)\Delta\tau} & = H_n(f_1)\cdot C_n(f_1) \end{cases} \tag{12}$$

where $H_1(f_1)$, $H_2(f_1)$, ..., $H_n(f_1)$, and $C_1(f_1)$, $C_2(f_1)$, ..., $C_n(f_1)$ represent the channel frequency response received from Link 1, Link 2, ..., Link N, and the system response (with the delay lines) of the Link 1, Link 2, ..., Link N, respectively. $\Delta\tau$ denotes the delay caused by the delay line and is related to the maximum propagation distance that can be detected. Due to the fact that the delay line is applied at IF signal, the delay caused by the delay line can be calculated as $\tau_{IF} = L_{delay}/c_{fiber}$, where $c_{fiber} = 2.04\times10^8$ m/s denotes the speed of the light in the optical fiber. The delay resolution for the IF signal is $\Delta\tau_{IF} = 1/BW_{IF}$, where BW_{IF} denotes the bandwidth of the IF signal. The delay resolution for the RF signal is $\Delta\tau_{RF} = 1/BW_{RF}$, where BW_{RF} is the bandwidth of the RF signal. Due to the fact that the signal we recorded is at RF frequency bands, we need to transform the delay line effect to the RF signal side. Thus, we can obtain the delay $\Delta\tau$ caused by the optical delay line as:

$$\Delta\tau = \frac{\tau_{IF}}{\Delta\tau_{IF}}\cdot\Delta\tau_{RF} = \frac{L_{delay}\cdot BW_{IF}}{c_{fiber}\cdot BW_{RF}} \tag{13}$$

Before the frequency response measurement, we record the system response $C_i'(f_1)$ of each multi-link individually in the

back-to-back connection, and $C_i^{'}(f_1)$ is recorded with the same frequency points, where i represents the index of the Rx link.

After using inverse discrete Fourier transform (IDFT), the impulse response $s(\tau)$ can be written as:

$$s(\tau) = s_1(\tau) + s_2(\tau - \Delta\tau) + \ldots + s_n(\tau - (N-1)\Delta\tau) \tag{14}$$

In the next step, we separate the impulse response into N parts equally by using a rectangular window function:

$$\begin{cases} s_1(\tau) & \approx [s_1(\tau) + \ldots + s_n(\tau - (N-1)\Delta\tau)] \cdot w(\tau) \\ s_2(\tau - \Delta\tau) & \approx [s_1(\tau) + \ldots + s_n(\tau - (N-1)\Delta\tau)] \cdot w(\tau - \tau_1) \\ & \vdots \\ s_n(\tau - (N-1)\Delta\tau) & \approx [s_1(\tau) + \ldots + s_n(\tau - (N-1)\Delta\tau)] \cdot w(\tau - (N-1)\tau_1) \end{cases} \tag{15}$$

where τ_1 is the separation delay index for the Link 1 and the window function $w(\tau)$ is:

$$w(\tau) = \begin{cases} 1 & \tau \in [0, \tau_1], \\ 0 & else \end{cases} \tag{16}$$

To avoid the calculation error, e.g. frequency point mismatch, as shown in (17), $C_i^{'}(f_1)$ is transformed to $c_i^{'}(\tau)$ by using the IDFT function and the same window function as (16) is used.

$$\begin{cases} c_1(\tau) & \approx c_1^{'}(\tau) \cdot w(\tau) \\ c_2(\tau - \Delta\tau) & \approx c_2^{'}(\tau) \cdot w(\tau - \tau_1) \\ & \vdots \\ c_n(\tau - (N-1)\Delta\tau) & \approx c_n^{'}(\tau) \cdot w(\tau - (N-1)\tau_1) \end{cases} \tag{17}$$

After the discrete Fourier transform (DFT), the channel frequency responses (CFRs) of the Rx links $H_1(f_1)$, $H_2(f_1)$, ..., $H_n(f_1)$ could be obtained as:

$$\begin{cases} H_1(f_1) & = \frac{S_1(f_1)}{C_1(f_1)} \\ H_2(f_1) & = \frac{S_2(f_1) \cdot e^{-j2\pi f_1 \Delta\tau}}{C_2(f_1)} \\ & \vdots \\ H_n(f_1) & = \frac{S_n(f_1) \cdot e^{-j2\pi f_1 (N-1)\Delta\tau}}{C_n(f_1)} \end{cases} \tag{18}$$

where $C_1(f_1)$,$C_2(f_1)$,...,$C_n(f_1)$ denote the system response in the frequency domain after using the window function in (16).

III. Channel Sounder Performance Validation

A. Link Budget Analysis

Fig. 5 illustrates the link budget of the developed phase-coherent channel sounder at 30 GHz as an example. Note that the link budget is analyzed for the back-to-back connection, which replaces the channels between the Tx and 2 Rxs with a splitter, as shown in Fig. 3. In this link budget analysis, 0.5 m RF cables and 300 m optical fiber cables are used. Note that in the back-to-back measurements and calibration process, an

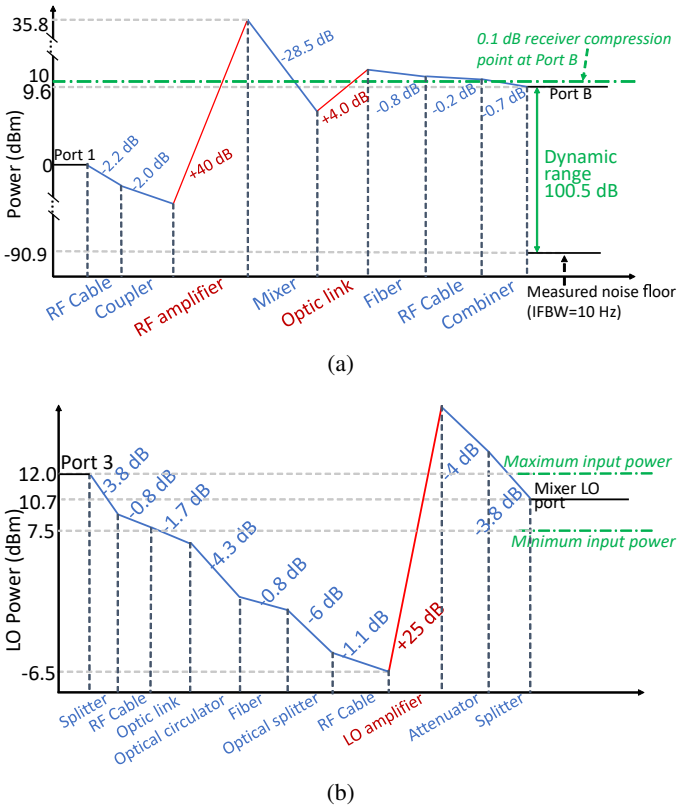

Fig. 5: Link budget in the back-to-back connection. (a) The proposed channel sounder at 30 GHz; (b) The phase compensation system at 10 GHz.

RF attenuator of 30 dB is used to avoid damage to the Rx mixers. In order to ensure that the system works safely and to prevent potential damage, the transmitted powers from Port 1 and Port 3 are 0 and 12 dBm, respectively. As shown in Fig. 5 (a), the coupler and the combiner have the insertion loss of 2 dB and 0.7 dB, respectively. Additionally, the LF optical link has a gain of 3.2 dB and the mixer causes a conversion loss of 28.5 dB at 30 GHz. Thus, the obtained dynamic range is 115.6 dB at 30 GHz for the back-to-back connection. Note that the noise floor of the VNA is specified for a VNA IF bandwidth of 10 Hz and is subject to the change depending on the VNA IF bandwidth settings.

For the phase compensation scheme, the link gain of the HF laser and photo detector is -1.7 dB. Besides, the optical circulators cause an associated insertion loss of 4.3 dB and the optical splitter has an RF power degradation of 6 dB. Thus, the phase compensation scheme causes a 12.8 dB signal loss for the forward link. To ensure that the mixer works in its normal region (i.e. input power in the range from $+7.5$ to $+12$ dBm), an RF amplifier operating at 2-18 GHz with a 25 dB gain and a 4 dB attenuator are employed resulting in 10.7 dBm LO power before the LO signal is fed to the Rx mixers.

B. Calibration Performance and Benchmarking

1) Calibration Performance: In this subsection, the procedure and validation results of the calibration are illustrated.

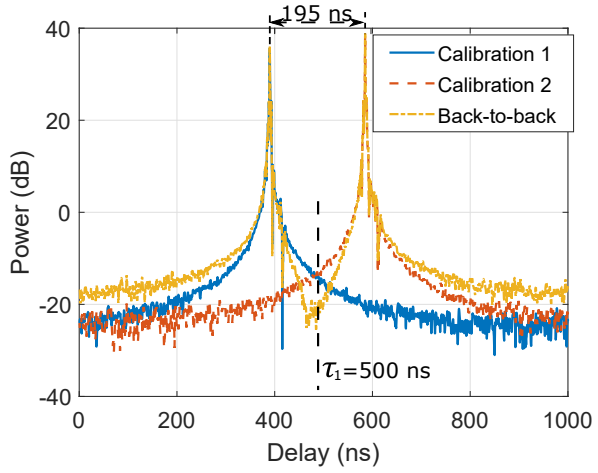

(a)

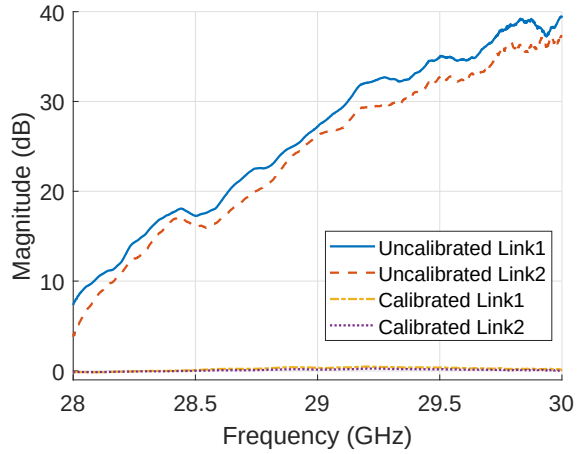

(b)

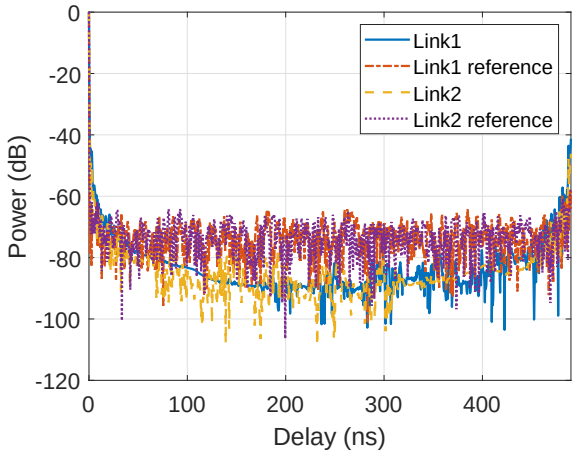

(c)

Fig. 6: CFR and CIR results. (a) Comparison of the CIR of the back-to-back and calibration; (b) CFR before and after calibration; (c) CIR for the Link 1 and the Link 2.

This calibration method is also validated by using two Rx links at 28-30 GHz with 2001 frequency points and 20 kHz VNA IF bandwidth in the back-to-back measurements. We used a 1632 m optical delay line on the Rx Link 2, while no delay line is used on Link 1 in this validation measurement. The channel is replaced with a one-to-two splitter in the back-to-back measurements. Note that to prevent the damage to the components, a 12-dB attenuator is used before the splitter. The measurement configurations are illustrated in Table II.

TABLE II: Simulation and measurement configuration for the sounder performance validation.

Parameter	Value	Parameter	Value
Simulation of the calibration procedure			
Frequency (GHz)	28-30	Delay line length (m)	20.4
Number of points	401	Power of Path 1 (dB)	20
Delay of Path 1 (ns)	10	Power of Path 2 (dB)	14
Delay of Path 2 (ns)	25		
Calibration performance			
Frequency (GHz)	28-30	Delay line length (m)	1632
Number of points	2001	VNA IF bandwidth (kHz)	20
Benchmark measurement			
Frequency (GHz)	20-23	Delay line length (m)	2000
Number of points	2001	VNA IF bandwidth (Hz)	10
Phase stability - signal drifting over time			
Frequency (GHz)	10-50	Delay line length (m)	2448
Number of points	32001	VNA IF bandwidth (kHz)	20
Total measured time (h)	8	Time interval (min)	1
Phase stability - cable bending			
Frequency (GHz)	28-30	Delay line length (m)	1632
Number of points	2001	VNA IF bandwidth (kHz)	20

As shown in Fig. 6 (a), in the delay domain, the two impulse response $s_1(\tau)$ and $s_2(\tau - \Delta\tau)$ could be clearly distinguished. Using (13), the measured $\Delta\tau_{meas} = 195$ ns are found to be close to the theoretical value $\Delta\tau_{theo} = (1632\,\text{m} \times 50\,\text{MHz})/(0.204\,\text{m/ns} \times 2\,\text{GHz}) = 200$ ns. Fig. 6 (b) shows the uncalibrated and calibrated CFR. The uncalibrated CFR magnitude for both links are observed to increase as the frequency increases, which is due to the increasing IF signal loss of the bias network at the Tx side with the increasing frequency. Furthermore, the calibrated CFRs are observed to be within 0.7 dB. Fig. 6 (c) illustrate the calibrated CIR for both links. Note that the reference CIR is the calibrated CIR by measuring the single link with 1001 frequency points and the same VNA IF bandwidth. Comparing the calibrated CFR with the uncalibrated CFR, and the calibrated CIR with the reference CIR in Fig. 6 (c), the results showed the feasibility and effectiveness of the proposed calibration procedure.

2) Benchmark measurement: In this subsection, a benchmarking measurement is conducted to validate the proposed channel sounder. The setup is similar with the back-to-back measurement in Section III-B1, i.e. using the one-to-two splitter and RF coaxial cables to replace the radio channel. Here we add a waveguide (Flann 22441) working at the frequency range of 21.5-40 GHz after the splitter in the link 2. A reference measurement is also conducted with the same measurement configurations by the simple VNA-based channel sounder, i.e. using two coaxial cables to connect the VNA and the waveguide. Note that before the reference measurement, the transmission normalization is performed to eliminate the system response of the two coaxial cables. Our purpose is

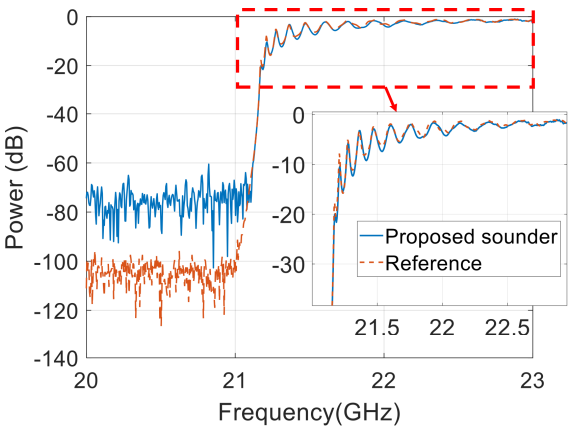

(a)

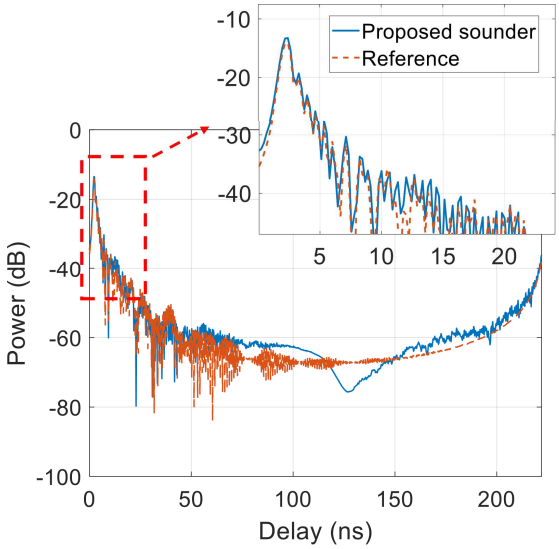

(b)

Fig. 7: Comparison of calibrated CFRs and CIRs of the waveguide in the benchmarking measurement. (a) Calibrated CFR; (b) Calibrated CIR.

to compare the calibrated CFR of the waveguide measured by our proposed sounder with the reference measurements to verify the effectiveness of our proposed channel sounder and calibration procedure. The measurement configurations of the benchmarking is illustrated in Table II.

Fig. 7 illustrates the calibrated CFRs and CIRs of the waveguide measured by the proposed sounder and the reference sounder, respectively. It can be observed that the calibrated frequency response of the proposed channel sounder in the frequency range of 21.1-23 GHz matches well with the reference, as depicted in Fig. 7 (a). However, noise floor of the proposed channel sounder in the frequency range of 20-21 GHz is different. The noise floor of the reference VNA-based channel sounder is -105 dB, while in our proposed channel sounder, the measured noise floor is -90.9 dB. Due to the use of the 12-dB attenuator, the dynamic range is reduced, which causes the noise floor difference in the measurement results. Fig. 7 (b) illustrates that the calibrated CIR of the proposed sounder matches well with the reference one. These measurement

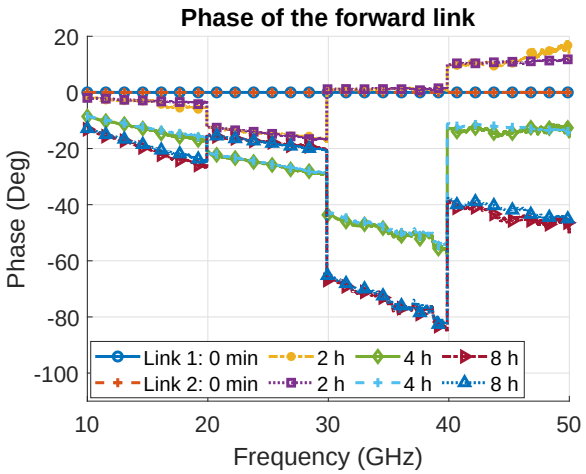

(a)

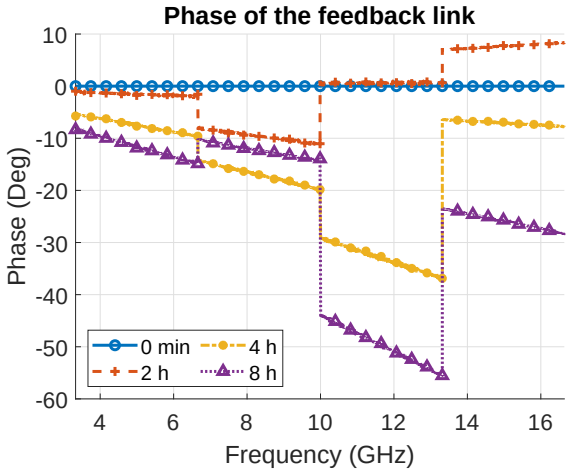

(b)

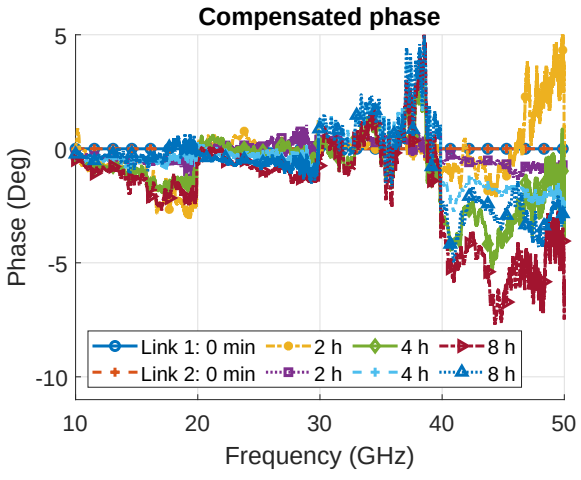

(c)

Fig. 8: Phase of the forward links and feedback link over a period of 8 hours. (a) Forward link;(b) Feedback link; (c) Compensated phase.

results demonstrate the feasibility and effectiveness of our proposed channel sounder.

C. Amplitude and Phase Stability Investigation

Amplitude and phase stability are fundamental if the channel sounder is to faithfully record the characteristics of the channel [19]. The proposed channel sounder is validated using back-to-back measurements. The amplitude and phase stability under the following two conditions are tested by the back-to-back measurements:

- signal drifting over time (thermal change);
- cable bending (mechanical stress).

1) Signal Drifting over Long Measurement Time: In practical VAA and directional scanning measurements at the Tx side or the Rx side, it could take several hours to record the channel responses. It is essential to ensure that there is insignificant signal drift in the measurement system during the entire measurement period. However, the subtle changes in the ambient temperature will cause a significant phase change to the signal in the optical fiber cable [19], [35]. To verify the robustness of our proposed channel sounder in the whole frequency range from 10-50 GHz, back-to-back measurements are required, as illustrated in Fig. 3. However, according to (13), due to the mixer limitation, if the RF bandwidth is set to be 40 GHz, $\Delta\tau$ would be extremely small (i.e. 10 ns using the 1632 m delay line) and the two signals are hard to be separated and distinguished. Thus, in these measurements, we verify the proposed channel sounder in four sub-bands with 10 GHz bandwidth (i.e. 10-20 GHz, 20-30 GHz, 30-40 GHz, and 40-50 GHz). The length of the delay line used in these measurements is 2448 m, corresponding to $\Delta\tau$ of 60 ns. During the measurements, a frequency sweep with the bandwidth of 10 GHz and the frequency points of 8001 is executed continuously for a period of 8 hours at an interval of 1 minute. Note that the VNA and the RF amplifier are firstly turned on and warmed up for 30 minutes before the measurements. The measurement configurations are illustrated in Table II.

The phase results from 10 to 50 GHz over a period of 8 hours are demonstrated in Fig. 8. In the phase of the forward link (i.e. without the compensation scheme), as illustrated in Fig. 8 (a), it is observed that the phase varies over 80° and is approximately 1.5 times the phase of the feedback link, as demonstrated in Fig. 8 (a) and (b). The measured phase ratio between the forward link and the feedback link is 1.5, which is consistent with the theoretical value, as depicted in (9) and (10). This demonstrates the effectiveness of the phase compensation scheme. Note that the reason for the phase jumping observed from Fig. 8 (a) and (b) is that the 4 measurements are not measured at the same time. The compensated phase deviation for the period of 8 hours is maintained within 3° at 10-30 GHz and 7° at 30-50 GHz, respectively, as illustrated in Fig. 8 (c). These results indicate the robustness and effectiveness of this proposed phase-compensated channel sounder in 8 hours.

2) Cable Bending: In practical directional scanning measurements, at the Rx side, mechanical stresses on the optical

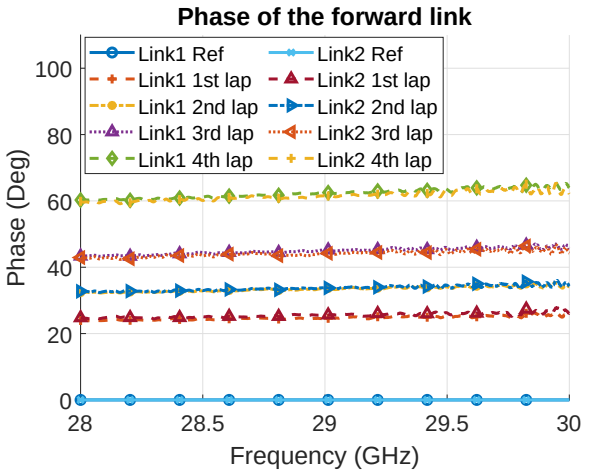

(a)

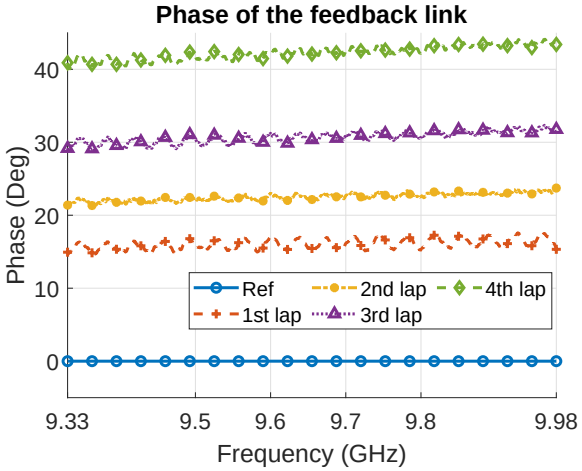

(b)

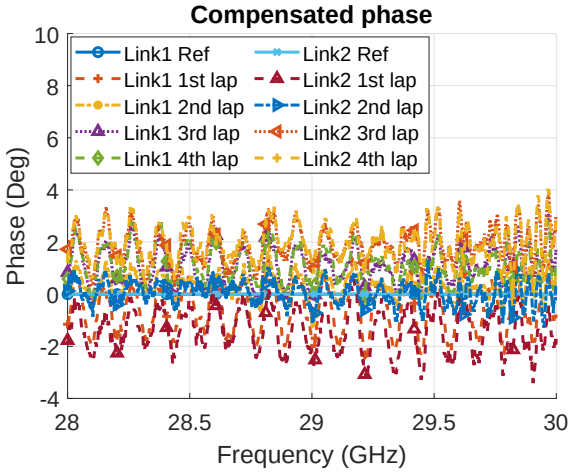

(c)

Fig. 9: Phase of the proposed channel sounder with cable bending. (a) Phase of the forward link for both two Rx links; (b) Phase of the feedback link; (c) Compensated phase for both two Rx links.

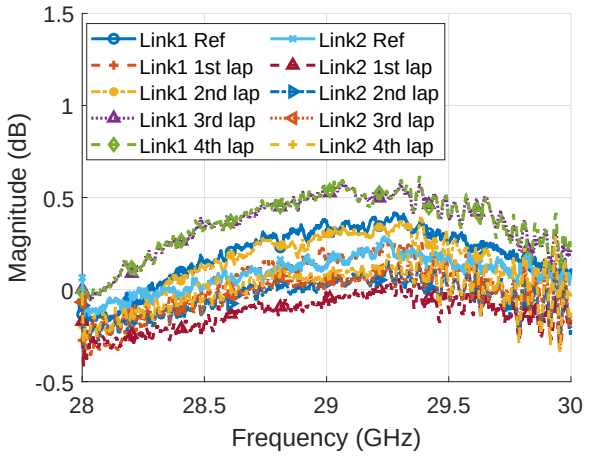

Fig. 10: Compensated amplitude of the channel sounder with cable bending.

fiber and Rx coaxial cables are inevitable due to the movement of the antenna positioning stages. To characterize the cable bending, a cylinder with a diameter of 28 cm is used to bend the cables. Then cable bending responses are measured for a total of 4 laps around the cylinder at 28-30 GHz. The measurement configurations are the same as the calibration validation measurements in Section II. C and are shown in Table II.

Fig. 9 and Fig. 10 illustrate the mechanical stress phase and amplitude results. Fig. 10 illustrates that the amplitude varies within 0.6 dB. As shown in Fig. 9 (a), the phase of the forward link is observed to be unstable as it varies over 60°. Compared with Fig. 9 (a) and Fig. 9 (b), the phase of the forward link is approximately 1.5 times the phase of feedback link as expected. After the phase compensation procedure, the phase due to mechanical stress is observed to be maintained within 4° at the frequency range of 28-30 GHz, as depicted in Fig. 9 (c), which clearly demonstrates the effectiveness of the phase compensation system.

D. Sounder Capability Discussion

In this subsection, the capability of the proposed channel sounder is discussed. The proposed channel sounder could enable cost-effective multi-link channel measurement operating at the frequency range from 10 to 50 GHz. The RoF techniques and the phase compensation scheme are applied to enable long-range phase-coherent measurements. Besides, the use of the optical delay line and combiner scheme saves the VNA port resource. The capabilities of our proposed channel sounder are summarized as follows:

- **Scalable frequency bandwidth.** With the use of the VNA and the suitable components, the ultrawideband channel measurement could be conducted in the frequency range from 10-50 GHz.
- **Long-range capability.** In this proposed channel sounder, the length of the fiber we used is 300 m. Thus, in principle, we can support channel sounding with a maximum measurement distance of 300 m. However, we need to consider over-the-air free space propagation loss and the antenna misalignment loss in the real measurement scenario. Moreover, the dynamic range of our proposed channel sounder is 100.5 dB, and according to the Friis free-space path loss (FSPL) formula (in decibel) at 30 GHz as:

$$FSPL = 20 * \log_{10}\left(\frac{4\pi f d}{c}\right) = 20 * \log_{10} d + 61.98, \tag{19}$$

where f, d, and c represent the frequency, the measurement distance, and the speed of light in vacuum, respectively. Assuming 4.5 dBi antenna gains for both Tx and Rx, which is the same as that of the commercial omnidirectional biconical antenna we used in Section IV, the theoretical maximum measurement range could reach 237.7 m at 30 GHz for the LoS scenario.
- **Phase-coherent measurement.** As mentioned in the introduction, the phase of the fiber is unstable at higher frequency bands, e.g. mmWave bands, which makes the RoF scheme unsuitable for phase-coherent measurements such as VAA. With the use of the phase compensation scheme, we could stabilize the phase in the post-processing. Thus, the phase-compensated RoF scheme could be used in phase-coherent measurements.
- **Saving port resource and cost-effectiveness.** As shown in Fig. 2, VNA has limited receiving ports and with the phase-compensated RoF scheme, the number of the multi-links is limited to 4. Due to the use of the delay line and combiner scheme, we could use one receiving port for more multi-links. Moreover, to apply the delay line and conduct long-range measurements, HF RoF scheme is required for each multi-link, which will increase the cost of the sounder. In our proposed channel sounder, the down-conversion system, i.e. mixers are utilized to down-convert the high frequency to low frequency, e.g. 10-50 MHz. In this way, we could apply LF RoF scheme to reduce the cost.

On the other hand, according to Fig. 2 and (13), the following aspects should be considered for the proposed channel sounder:

- **RF frequency range.** The RF frequency range of this sounder is limited by the working frequency of the mixer (i.e. 2-50 GHz). Furthermore, the operating frequency bands of the antenna and RF amplifier also limit the working frequency of this sounder, e.g. in the channel measurement section below, we use the antenna and RF amplifier operating at the frequency bands from 2-30 GHz and 26.5-40 GHz, respectively, which limits the channel measurements to the frequency range from 26.5-30 GHz.
- **IF signal bandwidth**. According to (13), the IF frequency bandwidth determines $\Delta\tau$, which is the key parameter to separate multi-links in the delay domain. The higher the IF frequency bandwidth, the longer the maximum propagation distance that could be detected. However, in the proposed sounder, due to the limitation of the 2-port mixer and the bias network, the IF frequency is limited within 10-60 MHz. By changing the 2-port mixer

and the bias network with the same 3-port mixer as that at the Rx side, the IF frequency range could be increased.

- **Delay line**. The length of the delay line is also the main factor to $\Delta\tau$. The delay line used in the validation is extremely long due to the narrow IF frequency bandwidth, the length of it could be shortened by increasing the IF frequency bandwidth, as explained in (13).
- **Number of frequency points**. The relationship between the number of frequency points M for the measurements and the number of Rx links N could be formulated as $M \geq m \times N$, where m denotes the number of frequency points for each Rx link. The RF bandwidth B_w and the number of frequency points for each Rx link m affects the maximum delay τ_{max} that can be resolved by the VNA as $\tau_{max} = m/B_w$. Since VNAs have a maximum number of frequency points, e.g. 100001 [27], the number of links N is typically limited by this. Moreover, a higher number of frequency points will lead to a longer sweeping time.
- **RF splitter used in the LO side and RF combiner**. As illustrated in Fig. 2, the maximum number of Rx links N_{max} also depends on the number of the output ports of the splitter in the LO side and the RF combiner. Increasing the Rx links, the number of ports for the splitter and combiner should be also increased. However, the signal loss on the splitter is also increased resulting in a decrease in the output power at the LO side.

Comparison of the proposed sounder and the state-of-the-art channel sounders is discussed as follows. The channel sounders in [15], [19], [20], [42], [43] are VNA-based channel sounders. A multi-link channel sounder is presented in [15] at $28\,$GHz with $4\,$GHz bandwidth. However, the measurement range of the sounder in [15] is limited to tens of meters due to the high signal loss in the cables, whereas our proposed sounder has a measurement range up to $237.7\,$m. RoF schemes are used in [42], [43] to extend the measurement range up to $100\,$m at mmWave and sub-Terahertz (sub-THz) frequency bands. However, due to the unstable phase performance of the fiber, the phase information of these channel frequency responses is inaccurate, which means that the high-resolution algorithms cannot be applied to the measurement data when the VAA concept is adopted. Phase-compensation scheme has been validated at 1-50 GHz in [19], [37], and at 300 GHz in [20], and the measurement results in those papers demonstrate the practicality and effectiveness of the phase compensation principle and structure. However, the phase compensation scheme is only validated in single-input-single-output channel sounders. Moreover, due to the high cost of the HF RoF units (i.e. HF laser and photo detector) and the port limitation of the VNA, it is impractical to directly extend the phase compensation scheme to multi-link or MIMO channel sounder. Thus, in this paper, we proposed a cost-effective phase-compensated long-range channel sounder using a minimal number of VNA ports. Using delay lines, signals from multiple links can be differentiated in the delay domain and then combined into a single port. In [38], a fast switch-based time-domain channel sounder using software-defined radio (SDR) hardware forming a 2×2 MIMO is proposed, which enables channel measurements with $160\,$MHz bandwidth and $5\,$ns measurement time for one CIR. However, the measurement frequency is at sub-$6\,$GHz, and the bandwidth is limited. In [44], a sliding-correlation-based channel sounder with the bandwidth of $1\,$GHz is presented. The time interval between two CIRs is $2\,$ms. The dynamic range is $48\,$dB for the dynamic short-range scenarios, and additional receiver architecture is required to obtain a higher dynamic range. To measure higher frequency bands, e.g. mmWave bands, these two channel sounders require additional up-and-down-converters. Moreover, synchronization becomes complicated and costly in long-range measurements. Compared to these two time-domain channel sounders, our proposed channel sounder could achieve a scalable frequency setting and bandwidth. Furthermore, the signal generator and analyzer are co-located in the VNA, which means that synchronization is not an issue in the VNA-based channel sounder. However, the slow frequency sweeping time limits the use of the proposed sounder in highly dynamic scenarios.

IV. Channel measurement validation

The proposed channel sounder is validated and measured in two realistic indoor propagation scenarios, i.e., indoor hall scenario and long corridor scenario. At the Tx and the Rx, vertically polarized biconical antennas are utilized. During the channel measurements, a 23×30 virtual uniform rectangular array (URA) (i.e. 690 array elements) with the inter-element spacing of 0.4λ is implemented at the Tx by using the high-precision positioning stage. This is done by mechanically moving the biconical antenna to multiple spatial locations following the array configuration of a URA. After the phase compensation and calibration procedure, the spatial-temporal channel characteristics are obtained using the classical beamforming algorithm due to its simplicity, robustness, and high spatial resolution offered by the large-scale VAA. Readers are referred to [15], [45] for the details of the classical beamforming principle. In both channel measurements, a 30-dB dynamic range is considered relative to the power of the line-of-sight (LoS) component.

A. Measurements in a hall

To evaluate the proposed channel sounder, the channel measurements at 28-30 GHz are firstly carried out in an indoor hall scenario, as illustrated in Fig. 11 (a). A frequency sweep from 28-30 GHz is performed with 1501 frequency points and $20\,$kHz VNA IF bandwidth for each virtual array element. Note that a larger VNA IF bandwidth is set for the VNA to save measurement time. The hall size is $8.2 \times 4.8\,\text{m}^2$. The antennas are fixed at the same height of $1.45\,$m. The link distances from the Tx to the Rx1 and the Rx2 are $4.1\,$m and $4.15\,$m, respectively, while the distance between the Rx1 and the Rx2 is $1\,$m. Note that the RF amplifier before the Tx antenna is removed in these measurements. Note that the RF cables used to connect the Rx mixer and the antenna for the Link 1 and Link 2 are $1\,$m and $2\,$m, respectively, which causes $4\,$dB dynamic range difference. A summary of the measurement configurations is outlined in Table III.

(a)

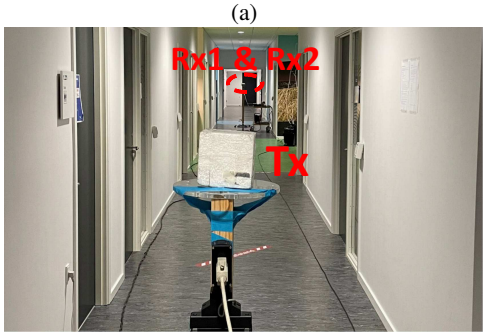

(b)

Fig. 11: Photos of the two channel measurement scenarios: (a) indoor hall scenario; (b) long corridor scenario.

TABLE III: Measurement configuration for the two scenarios.

Parameter	Indoor hall Value	Long-range corridor Value
Frequency (GHz)	28-30	29-30
Array size (x$\times y$)	23×30	
Inter-element distance (cm)	0.4	
Number of points	1501	
Transmitted power (dBm)	0	
VNA IF bandwidth (kHz)	20	
Antenna height (m)	1.45	
Tx antenna gain (dBi)	4.5	
Rx antenna gain (dBi)	5	
Length of the delay line (m)	1632	
RF amplifier gain (dB)	-	40

Fig. 12 depicts the exemplary measured CIRs before and after calibration. As shown in Fig. 12, the measured $\Delta\tau$ of 195 ns matches the theoretical value and the region from 0 to 320 ns is observed to be the noise. Thus, in this measurement, we choose Region 1 (i.e. $[250, 500]$ ns) and Region 2 (i.e. $[500, 750]$ ns) as the CIRs for Link 1 and Link 2, respectively. The maximum detecting delay for Link 1 and Link 2 is observed to be 164.5 and 219.5 ns, corresponding to the maximum detecting distance of 49.35 and 65.85 m, respectively. Fig. 13 (a) and (b) illustrate the power angular delay profiles (PADPs) of the both two links. The 6 dominant paths (i.e. path 1-6) and 5 weak paths (i.e. path 7-11) have been identified for the analysis for both two links. Due to the small range of the measurement scenario, the PADPs of Link 1 and Link 2 are observed to decay at approximately 36.5 ns and 42 ns, respectively. For Link 1, the LoS has an AoD of 171° and a delay of 13.5 ns, while for Link 2, the AoD and delay of the LoS path are 186° and 14 ns, respectively, which corresponds to the link distances between the Tx and the Rxs. The relationship between the identified

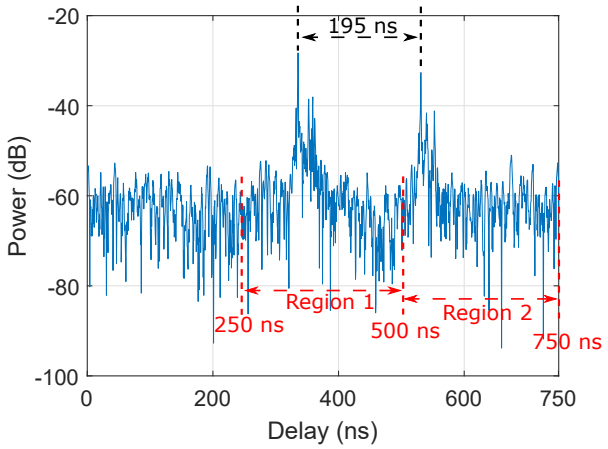

(a)

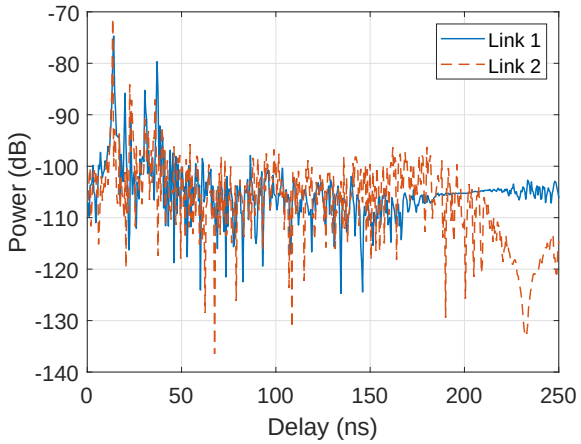

(b)

Fig. 12: An example of the measured CIR before and after calibration in the small-range hall scenario. (a) Before calibration; (b) After calibration.

multipath components (MPCs) and the room geometry are shown in Fig. 13 (c) and (d). For the paths of Link 1, path 2-6, 8, and 9 are concentrated in the AoD range of $[112°, 223°]$, while paths 7, 10, and 11 are MPCs originating from the back wall of the Tx. Meanwhile, path 3 and 5 of Link 2 are reflected from the door and metallic reflector, and paths 7-9, and 11 are reflected from the back wall of the Tx, whereas path 2, 4-6, and 10 are from the wall on both two sides. The one-to-one correspondence of the delay and AoD of the identified MPCs and the path trajectory of the room geometry demonstrate a good performance of the proposed channel sounder in this hall scenario.

B. Measurements in a long-range corridor

To validate the long-range capability of the proposed channel sounder, the channel measurements are performed in a long-range corridor scenario, as illustrated in Fig. 11 (b). A frequency sweep from 29-30 GHz is performed with 1501 frequency points and 20 kHz VNA IF bandwidth for each virtual array element. According to (13), we choose 1 GHz

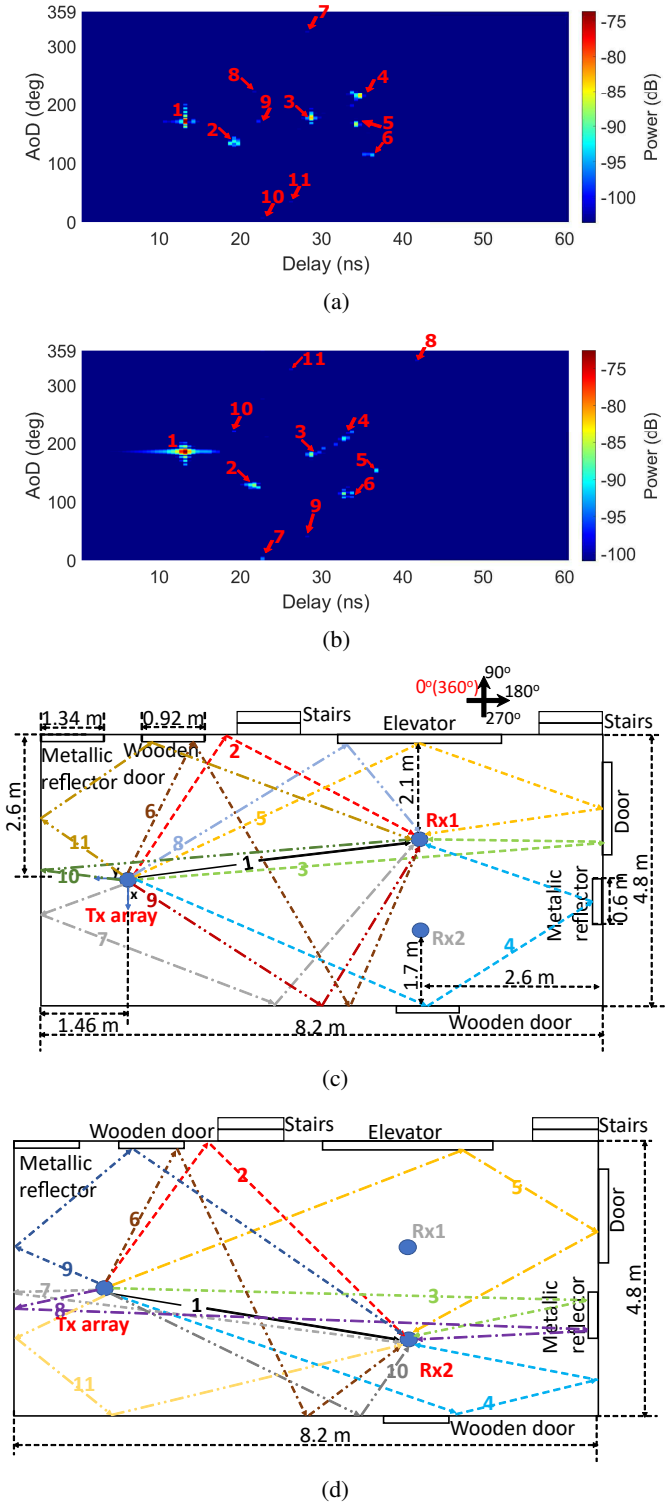

Fig. 13: Results of the channel measurements in the hall scenario: (a) PADP of Link 1; (b) PADP of Link 2; (c) Relation between the identified MPC and the scenario for Link 1; (d) Relation between the identified MPC and the scenario for Link 2.

RF frequency bands to reach a longer maximum detecting distance with the same length of the delay line. The length of the corridor is 43 m. The link distances from the Tx to Rx1 and from the Tx to Rx2 are 20.5 m and 23 m, respectively. The RF cables used in this measurement are the same as those in the hall scenario. The measurement configurations are illustrated in Table III.

Exemplary measured CIR before and after calibration are illustrated in Fig. 15. The measured $\Delta\tau$ of 400 ns matches the theoretical value, as shown in Fig. 15. Thus, Region 1 (i.e. $[500, 1000]$ ns) and Region 2 (i.e. $[1000, 1500]$ ns) are chosen as the CIRs for Link 1 and Link 2 in this measurement, respectively. The maximum detecting delay is observed to be 372 ns, corresponding to the maximum detecting distance of 111.6 m. PADPs of both two links are demonstrated in Fig. 14. The multipaths of both two links are mainly concentrated in the AoD range of $[160°, 202°]$ and $[-15°, 23°]$. The 9 dominant paths are identified for the analysis for Link 1 and 2. The PADPs of Link 1 and Link 2 are observed to decay at approximately 348 ns and 358 ns, corresponding to the propagation distances of 104.5 m and 107.4 m, respectively. For Link 1, the LoS has an AoD of 180° and a delay of 69 ns. Path 2, 4, 6, and 8 are seen to be the first-order reflection. Besides, path 5 and 7 are the second-order reflection. For Link 2, the AoD and delay of the LoS path are 180° and 78 ns, respectively, which correspond to the link distances from the Tx to the Rxs. Path 2, 4, 5, and 7 are observed to be the first-order reflection, while path 6, 8, and 9 are the second-order reflection. Furthermore, path 3 of Link 1 and Link 2 are observed to be third-order reflection. The relation of the main identified MPCs to the room geometry is shown in Fig. 16. The identified delay and angle information match well with the path trajectory, which demonstrates the long-range capability of the sounding system.

V. Conclusion

In this paper, a novel cost-effective multi-link long-range phase-compensated channel sounder at 10-50 GHz is proposed. The dynamic range of this channel sounder could be improved to 115.7 dB for the back-to-back connection at 30 GHz to support the long-range measurements. By using the phase-compensated RoF scheme, the long-range phase-coherent channel measurement could be conducted. The use of the optical delay lines and combiner could save the resource of the VNA ports, according to Section III-D, the number of the multi-links could reach 16 at mmWave bands by using one receiving port. Note that the multi-link number is not a limitation in our proposed channel sounder. Moreover, the down-conversion system, i.e. mixers, is utilized to demodulate the high frequency signal, e.g. mmWave to the low frequency, e.g. 10-50 MHz, and we could use the LF RoF scheme to reduce the cost of the channel sounder. The robustness of this novel channel sounder is validated and specified for the frequency range from 10 to 50 GHz by back-to-back measurements. The phase change before the compensation is over 80° phase change introduced by cable effect at 10-50 GHz, compared to within 3° and 7° of the compensated phases at

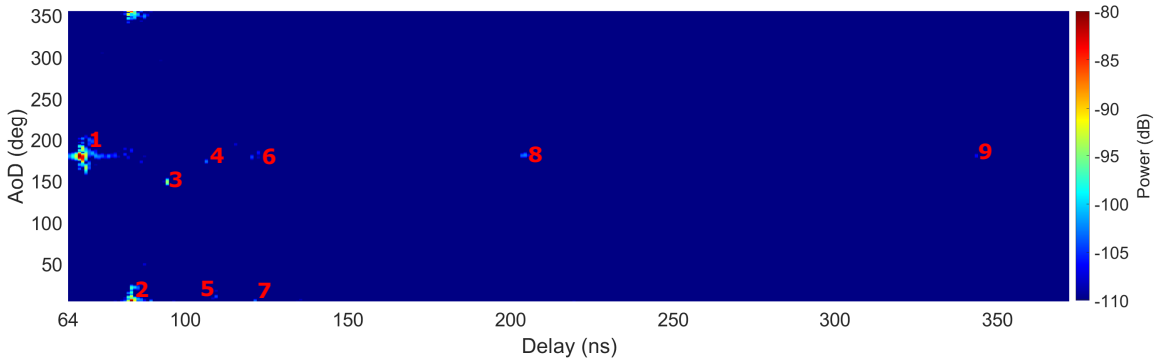

(a)

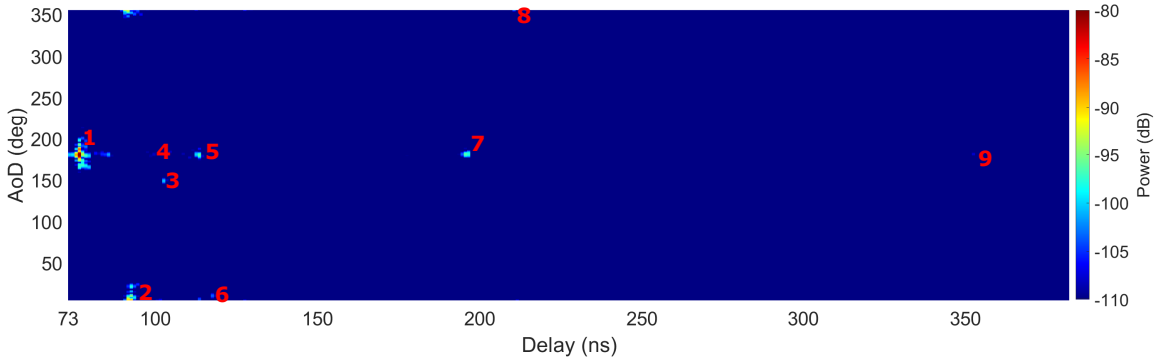

(b)

Fig. 14: PADPs of the channel measurements in the long-range scenario: (a) Link 1; (b) Link 2.

10-30 GHz and 30-50 GHz, respectively. Furthermore, channel measurements and analysis in the short-range hall scenario and long-range corridor scenario are carried out to validate and demonstrate the high fidelity of the proposed channel sounder.

REFERENCES

[1] E. G. Larsson, O. Edfors, F. Tufvesson, and T. L. Marzetta, "Massive MIMO for next generation wireless systems," *IEEE Communications Magazine*, vol. 52, no. 2, pp. 186–195, 2014.

[2] F. Boccardi, R. W. Heath, A. Lozano, T. L. Marzetta, and P. Popovski, "Five disruptive technology directions for 5G," *IEEE Communications Magazine*, vol. 52, no. 2, pp. 74–80, 2014.

[3] X. Zhao, X. Liang, S. Li, and B. Ai, "Two-cylinder and multi-ring GBSSM for realizing and modeling of vehicle-to-vehicle wideband MIMO channels," *IEEE Transactions on Intelligent Transportation Systems*, vol. 17, no. 10, pp. 2787–2799, 2016.

[4] Z. Ma, B. Ai, R. He, Z. Zhong, and M. Yang, "A non-stationary geometry-based MIMO channel model for millimeter-wave UAV networks," *IEEE Journal on Selected Areas in Communications*, vol. 39, no. 10, pp. 2960–2974, 2021.

[5] J. Zhang, Y. Zhang, Y. Yu, R. Xu, Q. Zheng, and P. Zhang, "3-D MIMO: How much does it meet our expectations observed from channel measurements?" *IEEE Journal on Selected Areas in Communications*, vol. 35, no. 8, pp. 1887–1903, 2017.

[6] J. O. Nielsen, W. Fan, P. C. F. Eggers, and G. F. Pedersen, "A channel sounder for massive MIMO and mmWave channels," *IEEE Communications Magazine*, vol. 56, no. 12, pp. 67–73, 2018.

[7] S. Rey, J. M. Eckhardt, B. Peng, K. Guan, and T. Krner, "Channel sounding techniques for applications in THz communications: A first correlation based channel sounder for ultra-wideband dynamic channel measurements at 300 GHz," in *2017 9th International Congress on Ultra Modern Telecommunications and Control Systems and Workshops (ICUMT)*, 2017, pp. 449–453.

[8] C. Gentile, A. F. Molisch, J. Chuang, D. G. Michelson, A. Bodi, A. Bhardwaj, O. Ozdemir, W. A. G. Khawaja, I. Guvenc, Z. Cheng, F. Rottenberg, T. Choi, R. Mller, N. Han, and D. Dupleich, "Methodology for benchmarking radio-frequency channel sounders through a system model," *IEEE Transactions on Wireless Communications*, vol. 19, no. 10, pp. 6504–6519, 2020.

[9] S. L. H. Nguyen, J. Medbo, M. Peter, A. Karttunen, K. Haneda, A. Bamba, R. D'Errico, N. Iqbal, C. Diakhate, and J.-M. Conrat, "On the frequency dependency of radio channel's delay spread: Analyses and findings from mmmagic multi-frequency channel sounding," in *12th European Conference on Antennas and Propagation (EuCAP 2018)*, 2018, pp. 1–5.

[10] X. Gao, O. Edfors, F. Rusek, and F. Tufvesson, "Massive MIMO performance evaluation based on measured propagation data," *IEEE Transactions on Wireless Communications*, vol. 14, no. 7, pp. 3899–3911, 2015.

[11] J. Flordelis, X. Gao, G. Dahman, F. Rusek, O. Edfors, and F. Tufvesson, "Spatial separation of closely-spaced users in measured massive multi-user MIMO channels," in *2015 IEEE International Conference on Communications (ICC)*, 2015, pp. 1441–1446.

[12] l. O. Martnez, E. De Carvalho, and J. d. Nielsen, "Towards very large aperture massive MIMO: A measurement based study," in *2014 IEEE Globecom Workshops (GC Wkshps)*, 2014, pp. 281–286.

[13] A. Karstensen, J. . Nielsen, P. C. F. Eggers, E. De Carvalho, G. F. Pedersen, M. Alm, and G. Steinbck, "Multi-user spatial consistency analysis of outdoor massive-mimo measurements," *IEEE Transactions on Antennas and Propagation*, pp. 1–1, 2021.

[14] J. Flordelis, F. Rusek, X. Gao, G. Dahman, O. Edfors, and F. Tufvesson, "Spatial separation of closely-located users in measured massive MIMO channels," *IEEE Access*, vol. 6, pp. 40 253–40 266, 2018.

[15] A. W. Mbugua, W. Fan, Y. Ji, and G. F. Pedersen, "Millimeter wave multi-user performance evaluation based on measured channels with virtual antenna array channel sounder," *IEEE Access*, vol. 6, pp. 12 318–12 326, 2018.

[16] J. Zhang, A. A. Glazunov, J. Yang, X. Chu, and J. Zhang, "An experimental study on indoor massive 3D-MIMO channel at 30-40 GHz band," in *2018 International Symposium on Antennas and Propagation*

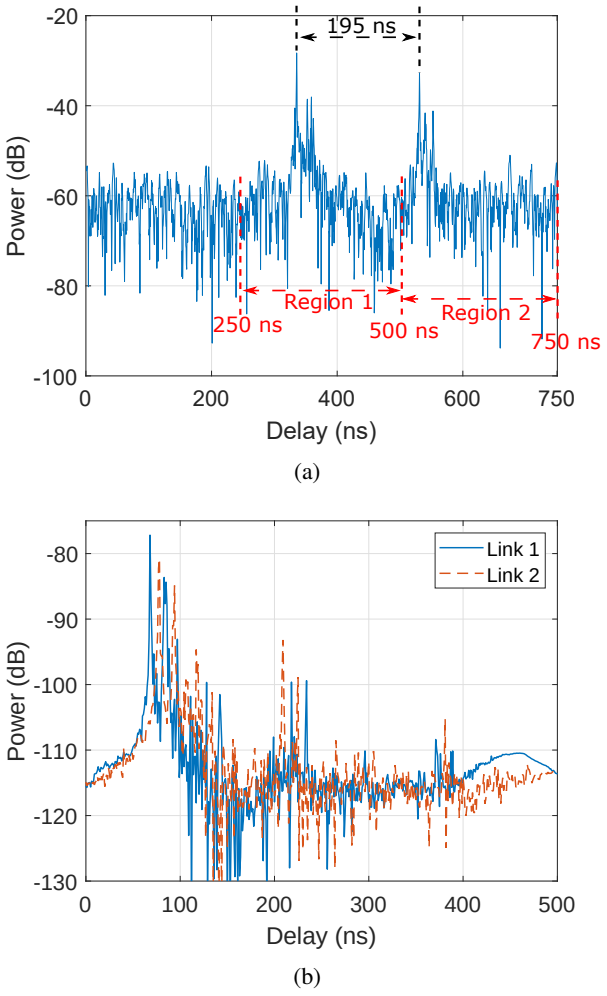

Fig. 15: An example of the measured CIR before and after calibration in the long corridor scenario. (a) Before calibration; (b) After calibration.

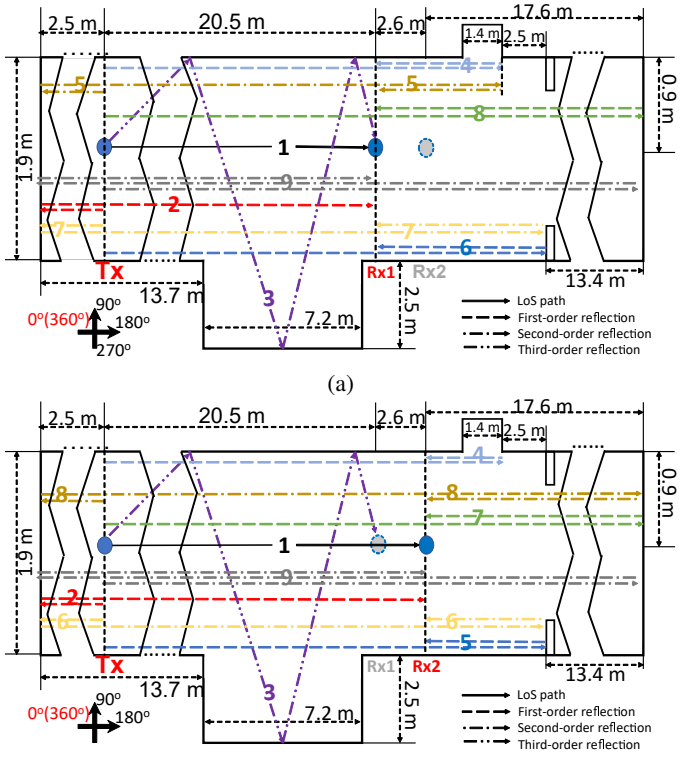

Fig. 16: Relationship between the identified MPCs and the corridor geometry for the long-range scenario: (a) Link 1; (b) Link 2.

(ISAP), 2018, pp. 1–2.

[17] A. Molisch, *Wireless communications*. John Wiley & Sons Ltd., 2011.

[18] J. Huang, C.-X. Wang, R. Feng, J. Sun, W. Zhang, and Y. Yang, "Multi-frequency mmwave massive mimo channel measurements and characterization for 5g wireless communication systems," *IEEE Journal on Selected Areas in Communications*, vol. 35, no. 7, pp. 1591–1605, 2017.

[19] A. W. Mbugua, W. Fan, K. Olesen, X. Cai, and G. F. Pedersen, "Phase-compensated optical fiber-based ultrawideband channel sounder," *IEEE Trans. Microw. Theory Techn.*, vol. 68, no. 2, pp. 636–647, 2020.

[20] Y. Lyu, A. W. Mbugua, K. Olesen, P. Kyosti, and W. Fan, "Design and validation of the phase-compensated long-range sub-THz VNA-based channel sounder," *IEEE Antennas and Wireless Propagation Letters*, pp. 1–1, 2021.

[21] B. Ai, K. Guan, R. He, J. Li, G. Li, D. He, Z. Zhong, and K. M. S. Huq, "On indoor millimeter wave massive MIMO channels: Measurement and simulation," *IEEE Journal on Selected Areas in Communications*, vol. 35, no. 7, pp. 1678–1690, 2017.

[22] H.-A. Nguyen, W. Keusgen, and T. Eichler, "Instantaneous direction of arrival measurements in mobile radio channels using virtual circular array antennas," in *2016 IEEE Globecom Workshops (GC Wkshps)*, 2016, pp. 1–7.

[23] D. Guven, B. F. Jamroz, J. Chuang, C. Gentile, R. D. Horansky, K. A. Remley, D. F. Williams, J. T. Quimby, A. J. Weiss, and R. Leonhardt, "Methodology for measuring the frequency dependence of multipath channels across the millimeter-wave spectrum," *IEEE Open Journal of Antennas and Propagation*, vol. 3, pp. 461–474, 2022.

[24] C. Gustafson, F. Tufvesson, S. Wyne, K. Haneda, and A. F. Molisch, "Directional analysis of measured 60 GHz indoor radio channels using SAGE," in *2011 IEEE 73rd Vehicular Technology Conference (VTC Spring)*, 2011, pp. 1–5.

[25] T. Zhou, C. Tao, S. Salous, and L. Liu, "Measurements and analysis of angular characteristics and spatial correlation for high-speed railway channels," *IEEE Transactions on Intelligent Transportation Systems*, vol. 19, no. 2, pp. 357–367, 2018.

[26] M. Li, F. Zhang, Y. Ji, and W. Fan, "Virtual antenna array with directional antennas for millimeter-wave channel characterization," *IEEE Transactions on Antennas and Propagation*, pp. 1–1, 2022.

[27] "Keysight VNA N5227B." [Online]. Available: https://www.keysight.com/en/pdx-2812784-pn-N5227B/pna-microwave-network-analyzer-67-ghz?&cc=DK&lc=dan

[28] "Rohde & Schwarz vector network analyzers." [Online]. Available: https://www.rohde-schwarz.com/us/products/test-and-measurement/network-analyzers/rs-zna-vector-network-analyzers_63493-551810.html

[29] X. Cai, G. Zhang, C. Zhang, W. Fan, J. Li, and G. F. Pedersen, "Dynamic channel modeling for indoor millimeter-wave propagation channels based on measurements," *IEEE Transactions on Communications*, vol. 68, no. 9, pp. 5878–5891, 2020.

[30] N. Zhang, J. Dou, L. Tian, X. Yuan, X. Yang, S. Mei, and H. Wang, "Dynamic channel modeling for an indoor scenario at 23.5 ghz," *IEEE Access*, vol. 3, pp. 2950–2958, 2015.

[31] J. Medbo, H. Asplund, J.-E. Berg, and N. Jalden, "Directional channel characteristics in elevation and azimuth at an urban macrocell base station," in *2012 6th European Conference on Antennas and Propagation (EUCAP)*, 2012, pp. 428–432.

[32] W. Stephens and T. Joseph, "System characteristics of direct modulated and externally modulated RF fiber-optic links," *Journal of Lightwave Technology*, vol. 5, no. 3, pp. 380–387, 1987.

[33] M. Mechaik, "Signal attenuation in transmission lines," in *Proceedings of the IEEE 2001. 2nd International Symposium on Quality Electronic Design*, 2001, pp. 191–196.

[34] F. Zhang, X. Ge, B. Gao, J. Wei, and S. Pan, "Phase stable radio

distribution over optic cable by phase conjugation using an optical frequency comb," in *2015 International Topical Meeting on Microwave Photonics (MWP)*, 2015, pp. 1–4.

[35] M. Calhoun, S. Huang, and R. L. Tjoelker, "Stable photonic links for frequency and time transfer in the deep-space network and antenna arrays," *Proceedings of the IEEE*, vol. 95, no. 10, pp. 1931–1946, 2007.

[36] W. Fan, A. W. Mbugua, and K. Olesen, "Accurate channel sounding with a phase stabilizing scheme," in *2020 XXXIIIrd General Assembly and Scientific Symposium of the International Union of Radio Science*, 2020, pp. 1–4.

[37] A. W. Mbugua, W. Fan, X. Cai, Y. Chen, W. Wang, K. Olesen, and G. F. Pedersen, "System development and experimental validation of a long-range vna-based channel sounder," *IET Microwaves, Antennas & Propagation*, vol. 14, no. 14, pp. 1733–1741, 2020.

[38] D. Stanko, G. Sommerkorn, A. Ihlow, and G. del Galdo, "Enable software-defined radios for real-time MIMO channel sounding," in *2021 IEEE International Instrumentation and Measurement Technology Conference (I2MTC)*, 2021, pp. 1–5.

[39] S. Mahboob and S. B. Ram, "Vector channel-sounder using fiber delay lines to separate the channels," in *2017 IEEE International Symposium on Antennas and Propagation USNC/URSI National Radio Science Meeting*, 2017, pp. 1113–1114.

[40] M. F. De Guzman, M. Hassan, and K. Haneda, "Uncertainty of millimeter-wave channel sounder due to integration of frequency converters," in *2021 17th International Symposium on Wireless Communication Systems (ISWCS)*, 2021, pp. 1–6.

[41] S. S. Zhekov, A. Tatomirescu, and G. F. Pedersen, "Antenna for ultra-wideband channel sounding," *IEEE Antennas and Wireless Propagation Letters*, vol. 16, pp. 692–695, 2017.

[42] J. Vehmas, J. Jarvelainen, S. L. H. Nguyen, R. Naderpour, and K. Haneda, "Millimeter-wave channel characterization at Helsinki airport in the 15, 28, and 60 GHz bands," in *2016 IEEE 84th Vehicular Technology Conference (VTC-Fall)*, 2016, pp. 1–5.

[43] N. A. Abbasi, A. Hariharan, A. M. Nair, A. S. Almaiman, F. B. Rottenberg, A. E. Willner, and A. F. Molisch, "Double directional channel measurements for THz communications in an urban environment," in *ICC 2020 - 2020 IEEE International Conference on Communications (ICC)*, 2020, pp. 1–6.

[44] G. R. MacCartney and T. S. Rappaport, "A flexible millimeter-wave channel sounder with absolute timing," *IEEE Journal on Selected Areas in Communications*, vol. 35, no. 6, pp. 1402–1418, 2017.

[45] H. Krim and M. Viberg, "Two decades of array signal processing research: the parametric approach," *IEEE Signal Processing Magazine*, vol. 13, no. 4, pp. 67–94, 1996.